

# The Selection and performance of Diamond Radiators used in Coherent Bremsstrahlung Experiments

J.D. Kellie<sup>a</sup> P.J.M. Clive<sup>a</sup> G.L. Yang<sup>a</sup> C. Gordon<sup>a</sup> C. Hall<sup>e</sup>  
J. W. Harris<sup>b</sup> R.T.Jones<sup>f</sup> K. Livingston<sup>a</sup> I.J.D. MacGregor<sup>a</sup>  
J.C. McGeorge<sup>a</sup> J. Melone<sup>a</sup> R.O.Owens<sup>a</sup> P.A. Slaven<sup>d</sup>  
R.M. Vrceelj<sup>c</sup> D. Watts<sup>g</sup>

<sup>a</sup>*Dept. of Physics and Astronomy, University of Glasgow, Glasgow, Scotland*

<sup>b</sup>*Division of Earth Sciences, University of Glasgow, Glasgow, Scotland*

<sup>c</sup>*Pfizer Institute for Pharmaceutical Material Science, University of Cambridge, England*

<sup>d</sup>*University of Strathclyde, Glasgow, Scotland*

<sup>e</sup>*Element 6, The Netherlands*

<sup>f</sup>*University of Connecticut, Storrs, CT, USA*

<sup>g</sup>*Dept. of Physics, University of Edinburgh, Edinburgh, Scotland*

---

## Abstract

The bremsstrahlung emitted as a result of scattering electrons in thin diamond crystals provides a useful source of high energy photons for use in photonuclear experiments, since the coherent bremsstrahlung produced is linearly polarized. Techniques for selecting the most favourable diamonds have been investigated. These are optical crossed polaroid analysis, X-ray topography and rocking curve measurements. The diamonds are characterised with a view to determining their performance as radiators, and bremsstrahlung spectra from a diamond radiator used at the Mainz MAMI-B facility are presented. The changes caused by high energy electrons to the crystal properties of the diamond and to the resulting coherent bremsstrahlung spectra are discussed.

*Key words:* Bremsstrahlung; Diamonds; Coherent Bremsstrahlung; Photonuclear studies

---

## 1 Introduction

A well established method for creating a beam of high energy linearly polarised photons for use in photonuclear studies is coherent bremsstrahlung production (1). The primary electron beam is scattered in a crystal whose regular lattice of atoms allows the recoil momentum to be taken up by the crystal as a whole, rather than by individual atoms. This occurs when the crystal is set at an angle to the incident electron beam such that the recoil momentum is equal to one of the crystal reciprocal lattice vectors, in a manner analogous to Bragg scattering.

In comparison to an incoherent bremsstrahlung spectrum from an amorphous radiator, a coherent bremsstrahlung spectrum has additional structure. Typical measured and calculated coherent and incoherent bremsstrahlung spectra are compared in figure 1. The solid black curves show the total measured photon energy spectra from nickel (top) and diamond (bottom). The dashed curves show theoretical fits to the data. (2). Figure 2 shows the total photon spectrum from a diamond divided by the spectrum from an amorphous radiator for the same electron beam energy. i.e. the relative intensity. The theoretical fit is shown as a dashed curve. For both figures 1 and 2 the fits are very good since it is difficult to distinguish them from the data points over most of the photon energy range. The strongest peak in the spectrum in figure 2 ( at  $\sim 280$  MeV) arises from the (220) crystal planes and the sharp decrease in intensity at the upper side of this peak will be referred to as the 'coherent edge'. The spectrum in figure 2 is normalized to have a value of 1 at the minimum of the edge. The structures at higher energy are due to the scattering from different crystal planes.

The main advantage of coherent bremsstrahlung is that the photons are linearly polarised. For example in the photon energy region where the intensity enhancement is greatest, the degree of linear polarisation can exceed 80% if the photon beam is suitably collimated. Diamond is particularly suitable as a radiator due to its high Debye temperature, which means that the amplitude of the thermal motion of the atoms in the lattice is small and the lattice structure is relatively unaffected by thermal effects. (3; 4).

Since diamond specimens always suffer from imperfections, one of the aims of the present study has been to find the extent to which they can be tolerated in coherent bremsstrahlung experiments. This can then be used as the basis for selecting suitable specimens. Ideally, the assessment technique should be simple and inexpensive but provide sufficient information to determine how well the diamond will perform as a radiator.

Diamonds are classified into four types, referred to as Ia, Ib, IIa and IIb (5). Type I have concentrations of nitrogen impurity varying from around 1 ppm. to greater than  $10^3$  ppm. The nitrogen in type Ia occurs in aggregated form, that is, the nitrogen atoms occur in the lattice in pairs, groups of four, or as part of other complexes formed with vacancies. In type Ib the nitrogen atoms

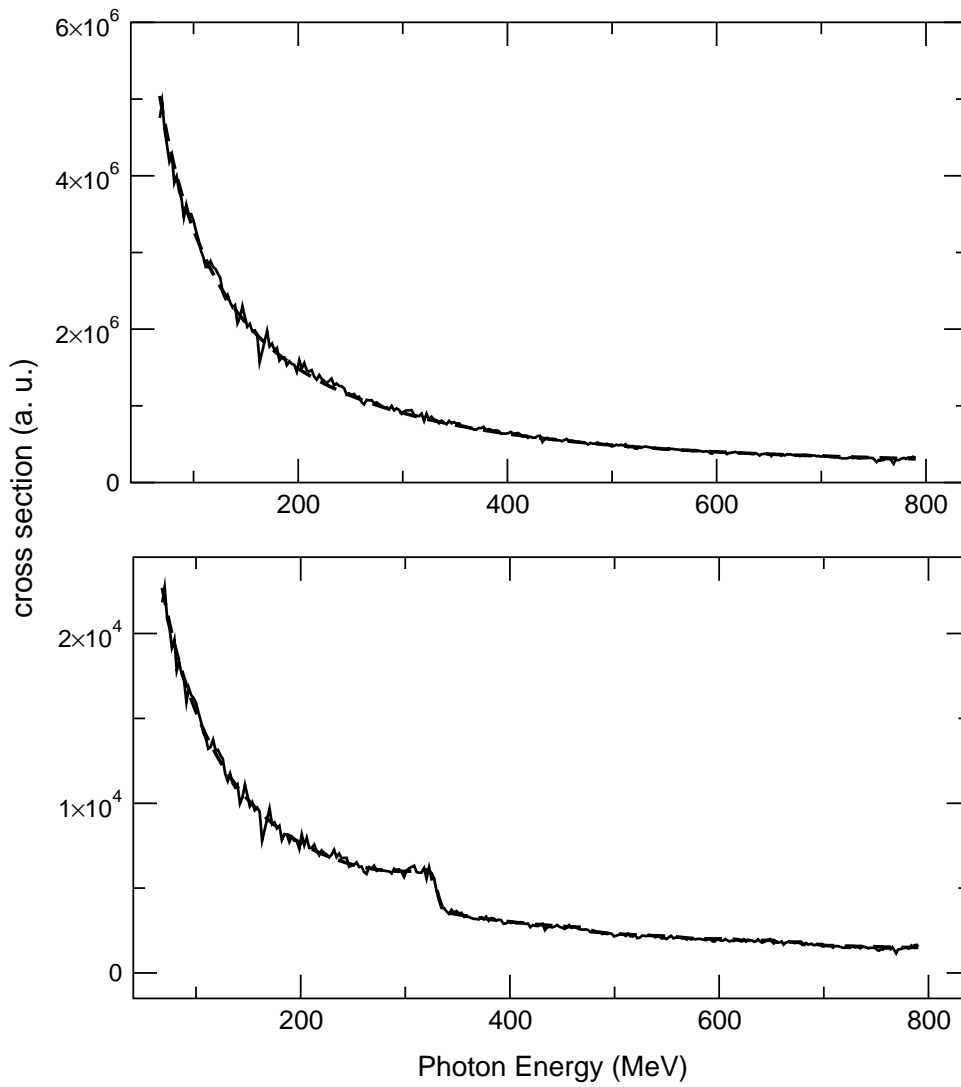


Fig. 1. Comparison of measured data (black line) and the theoretical least squares fit (dashed line) for the bremsstrahlung intensity for nickel (top) and diamond (bottom)

are substitutional and dispersed evenly through the volume of the diamond. Type II diamonds contain much less nitrogen than type I, in general less than 1 *ppm*. For natural diamonds, type II specimens are most probably the result of slow diamond growth. In the present paper both natural and synthetic industrial diamonds are assessed.

When an electron beam passes through a diamond radiator there is a spread in the direction of the electrons with respect to the crystal orientation due to three main causes; the divergence of the primary electron beam, multiple scattering of the electrons in the diamond and finally the variation in the crystal lattice arising from crystal defects. This angular variation degrades the coherent spectrum and it should be kept smaller than the bremsstrahlung

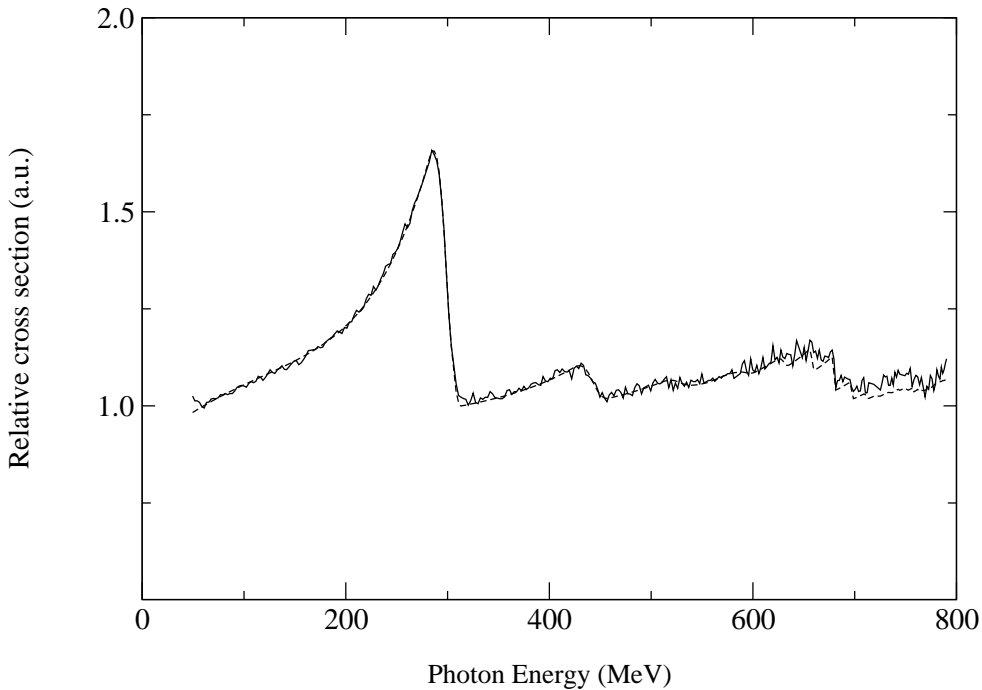


Fig. 2. Relative bremsstrahlung spectrum

characteristic opening angle,

$$\theta_{br} = \frac{mc^2}{E_0}$$

where  $m$  is the electron mass and  $E_0$  the incident electron beam energy. Since the present paper presents coherent bremsstrahlung spectra measured using the Glasgow tagged photon spectrometer (6; 7) at the 855 *MeV* electron accelerator in Mainz, we shall concentrate on coherent bremsstrahlung production at 855 *MeV*. We shall also discuss the production at 12 *GeV* since this will be relevant for the planned new experiment GlueX at the Jefferson Laboratory (8) which will use linearly polarized photons from coherent bremsstrahlung with a 12 *GeV* beam.

A change in the orientation of the diamond with respect to the incident electron beam causes the coherent edge to shift. Figure 3 shows the magnitude of the shift for the coherent peak produced by the 220 reciprocal lattice vector for  $E_0 = 855$  *MeV* and  $E_0 = 12$  *GeV* for a range of values of  $k = E_\gamma/E_0$  where  $E_\gamma$  is the bremsstrahlung photon energy. Indicated by the dashed lines are the shifts for  $E_\gamma \sim 240$  *MeV*, which is the coherent edge energy for measurements at Mainz which are discussed later in this paper, and for  $E_\gamma = 8$  *GeV*, which will be a typical energy for investigating the production of exotic hybrid mesons at GlueX (8). From figure 3 we find a change of magnitude of  $\theta_{br}$  in the electron direction causes the energy of the coherent peak produced by the 220 reciprocal lattice vector to change by  $\sim 2\%$  and  $\sim 0.4\%$  of  $E_0$  for

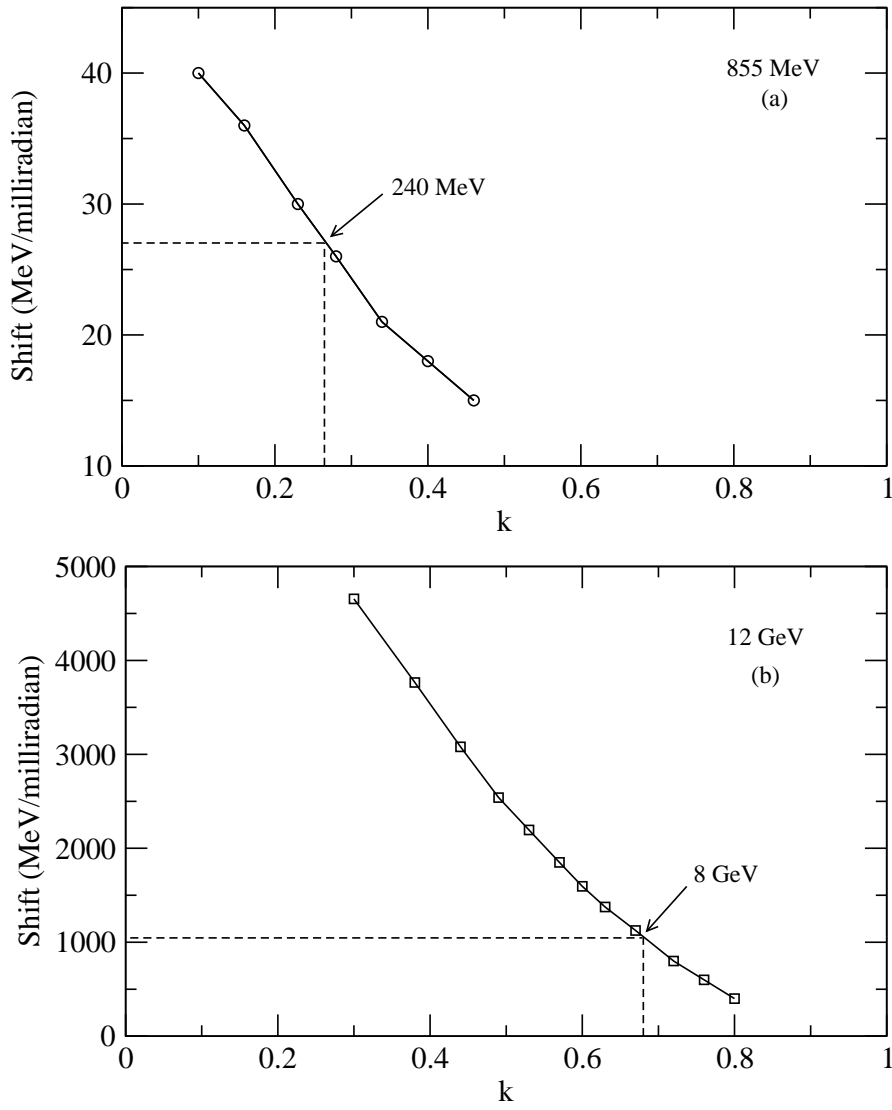


Fig. 3. Shift in position of the coherent edge from the 220 reciprocal lattice vector with respect to diamond orientation ( $MeV/milliradian$ ) for beam energies of 855  $MeV$  and 12  $GeV$  as a function of  $k = \frac{E_\gamma}{E_0}$ .

the energies  $E_\gamma = 240 MeV$  and 8  $GeV$  discussed above. It follows that an electron angular distribution of this magnitude will broaden the structure of the coherent peak and reduce the maximum polarization. The values of  $\theta_{br}$  for the Mainz and Jefferson Laboratory accelerators are around 600  $\mu rad$  and 40  $\mu rad$  respectively. Since the average divergence of the electron beam at Mainz is around 40  $\mu rad$  (9) and at the Jefferson Laboratory will be around 12  $\mu rad$  (8), the effect of beam divergence on the coherent bremsstrahlung spectra is or will be small for both laboratories.

Considering the spatial distribution of electrons undergoing multiple scattering, a reasonable approximation for the r.m.s. electron multiple scattering

angle is given by(10):

$$\theta_{sc} = \frac{19.2}{E_0} \sqrt{t} \times (1 + 0.038 \ln(t))$$

where  $E_0$  is expressed in MeV and  $t$  is the radiator thickness in radiation lengths. We find, the ratio:

$$\frac{\theta_{sc}}{\theta_{br}} = \frac{19.2}{mc^2} \sqrt{t} \times (1 + 0.038 \ln(t))$$

is independent of  $E_0$ , and hence a radiator of a given thickness will provide coherent bremsstrahlung spectra for which the effects of multiple scattering are equivalent at different beam energies. A reasonable upper limit for which the spreading of the coherent peak and the reduction in the polarization are small, is

$$\theta_{sc} = \frac{\theta_{br}}{2}.$$

This requires a diamond of thickness  $\sim 40 \mu m$ , which is  $3.6 \times 10^{-4}$  radiation lengths.

The final point affecting the spread in the direction of the electrons with respect to crystal orientation depends on the occurrence of crystal defects. This is addressed by trying to obtain specimens which ideally would be diamond monocrystals. Section 2 describes the techniques used to identify specimens with highly regular lattices.

## 2 Apparatus and Methods

The samples discussed in this paper were chosen to illustrate some of the common features found in diamond wafers and also to compare different types of diamond. The samples have thicknesses between 50 and 120  $\mu m$ . The details are given in table 1.

In characterising the diamonds to determine criteria for selecting the most suitable specimens to use as radiators in coherent bremsstrahlung experiments, three techniques have been used. The first is petrographic microscopy in which the diamonds are illuminated from below using polarised light, and then viewed from above through another polaroid, crossed perpendicular to the polaroid below, such that only areas where local birefringence in the crystal caused by strain fields associated with defects can be seen.

List of Diamond Specimens Investigated					
<i>Sample</i>	<i>Type</i>	<i>Thickness</i> ( $\mu m$ )	<i>Thickness</i> ( <i>rad. lengths</i> )	<i>Plane</i>	<i>Synthetic/</i> <i>Natural</i>
1	Ib	100	$8 \times 10^{-4}$	(001)	Synthetic
2	Ib	50	$4 \times 10^{-4}$	(001)	Synthetic
3	Ib	120	$10 \times 10^{-4}$	(011)	Synthetic
4	Ib	110	$9 \times 10^{-4}$	(001)	Synthetic
5	IIa	50	$4 \times 10^{-4}$	(001)	Natural
6	Ib	100	$8 \times 10^{-4}$	(001)	Synthetic

Table 1

A listing of the samples used in this survey.

The second and third techniques allow the defects to be studied with better resolution using X-rays. The first of these is X-ray topography, in which an image of the sample is obtained from a scattered parallel beam of X-rays. Variations in the lattice parameters of the crystal caused by the presence of defects result in contrast in the image.

Although the X-rays are scattered according to Bragg's law, the scattered intensity is not a delta function when plotted against the angle the crystal makes with the X-ray beam. Rather, there is a range of angles over which coherent scattering occurs for a given set of crystal planes, and the plot of the scattered intensity over this range of angles is known as a rocking curve (11; 12).

In the present paper, apart from a series of rocking curves for a sample which has suffered extensive damage from an 855 MeV electron beam, we present only transmission topographs and rocking curves for which the scattering planes in the diamond are at right angles to the surface of the diamond. Theoretical investigations ref(????), based on a dynamical treatment of X-ray scattering which takes into account dispersive effects inside the crystal, show that part of the diffracted X-ray amplitude is only minimally attenuated in passing through the crystal. Consequently, transmission topographs and rocking curves sample the whole volume of the diamond being studied. For the radiation damaged diamond, reflection rocking curves, in which the scattering planes are parallel to the surface of the diamond, are presented. If effects arising from its lattice structure are discounted, the absorption of X-rays in a crystal is described in terms of the linear attenuation coefficient  $\mu$  and the extinction length  $\frac{2}{\mu}$ . For diamond at a wavelength of  $1.54 \text{ \AA}$ , which is similar to the wavelengths used in the present investigations,  $\mu = 1.62 \times 10^3 m^{-1}$  and the extinction length is  $1.23 mm$ . Since the thickness of the radiation damaged diamond is  $100 \mu m$ , in terms of the linear attenuation coefficient, the X-rays can easily sample the whole volume of the diamond. However, the reflection

and transmission of X-rays through a perfect crystal can be significantly affected by both primary extinction, where interference can occur between the incident and diffracted beams, and secondary extinction where the removal of energy from the incident beam to the diffracted beam is taken into account. The importance of both primary and secondary extinction is substantially reduced if the crystal is non-perfect (13). Since this is certainly the case for the radiation damaged diamond, the reflection rocking curves still sample the whole volume of the diamond.

A rocking curve measurement is sensitive to crystal quality since it can determine the mosaic spread of the crystal. According to the mosaic model (14), an imperfect crystal is believed to be composed of a large number of small mosaic blocks; within each block the distribution of the atoms is perfect, but for different blocks, the crystal planes have different orientations. Usually it is assumed the mosaic angular distribution is Gaussian. The mosaic spread ( $\sigma_{mosaic}$ ) is the square root of the variance of the orientation distribution. If it is assumed the rocking curve also has a Gaussian distribution, the mosaic spread can be estimated from the rocking curve width; ie the  $FWHM = 2.35 \times \sigma_{mosaic}$ . The measurement of rocking curve widths is the third technique adopted.

Although the X-rays are scattered by atomic electrons, whereas the electrons in coherent bremsstrahlung are scattered by atomic nuclei, both processes are governed by the regularity of the lattice. Any deviations from this regularity, made apparent by the rocking curve width exceeding its theoretical value (see section 3), indicate the presence of crystal imperfections or regions of stress within the crystal. In the present paper we examine whether there are any identifiable changes to the coherent bremsstrahlung spectrum from a diamond having a broadened rocking curve. In particular, as mentioned above, a series of coherent bremsstrahlung spectra from a radiation damaged diamond which exhibits very large variations in rocking curve widths across the damaged region have been examined. The spectra were obtained at the MAMI-B Mainz microtron. The electron beam was passed through each crystal sample and the energies of the residual electrons measured using the Glasgow tagged photon spectrometer (6; 7). The photon energy spectrum was obtained directly from the residual electron energy spectrum. The diamond wafers were aligned relative to the electron beam according to the technique developed by Livingston (15).

The X-ray facility used was the synchrotron radiation source at Daresbury Laboratory, England. The experimental station lies at the end of an 80 m beam line ensuring that with adequate collimation the beam is effectively parallel. The topographs were obtained by exposing the whole area of the diamond samples to the main X-ray beam in transmission geometry and recording the scattered intensity using photographic plates positioned at the Bragg angle. For the rocking curves, a double crystal diffractometer set-up was used. Collimated monochromatic X-rays from a silicon crystal monochromator in the main X-ray beam, were scattered from the diamond samples and detected using a NaI counter. A (+,-) configuration was adopted in which the scattering



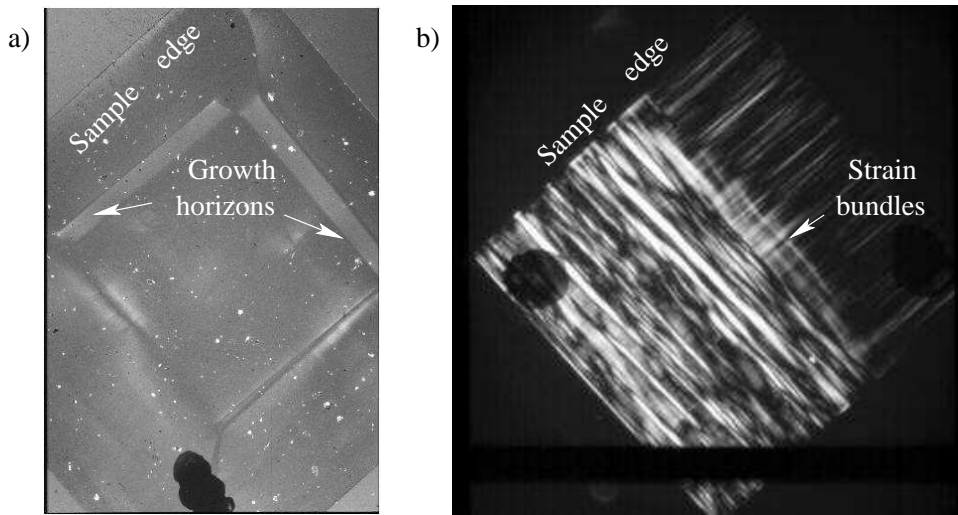


Fig. 4. Polarised light analyses of a) sample 1 and b) sample 5.

from the monochromator and the diamonds was in opposite directions. Section 3 presents petrographic images, topographs and rocking curves as well as measurements of coherent bremsstrahlung spectra from a variety of diamond radiators.

### 3 Results

Figure 4 shows the polarised light analyses of samples 1 and 5 and compares a synthetic type I with a natural type II. The black spots on figure 4(a) and 4(b) are identification marks. The black horizontal band at the bottom of 4(b) is an artifact of the photograph. Figure 4(a) shows an image of sample 1 taken with polarised light. It is virtually featureless, apart from some growth horizons, where strain has been induced due to differential growth rates on different families of crystal planes. There is also some dust on the surface of the diamond. Figure 4(b) shows an image of sample 5 taken with polaroids crossed at  $90^\circ$ . It shows bundles of linear features corresponding to line defects created as a result of the diamond undergoing plastic deformation in the Earth's upper mantle. The presence of these bundles of linear defects, sometimes referred to as a braided strain pattern, is typical of natural type II samples.

Figure 5 shows the transmission topographs and rocking curves of samples 1, 2 and 3, which are all type I industrial synthetic diamonds. The two vertical white lines on the topograph for sample 1 are due to the supporting wires for the sample. There is a clear similarity between the polarised light image and the topograph for sample 1. Due to its mounting, the light image is rotated by  $45^\circ$  with respect to the topograph but both show a central, approximately square, rather featureless region surrounded by growth horizons. Samples 1 and 2 are cut along (001) planes while sample 3 is cut along (011) planes

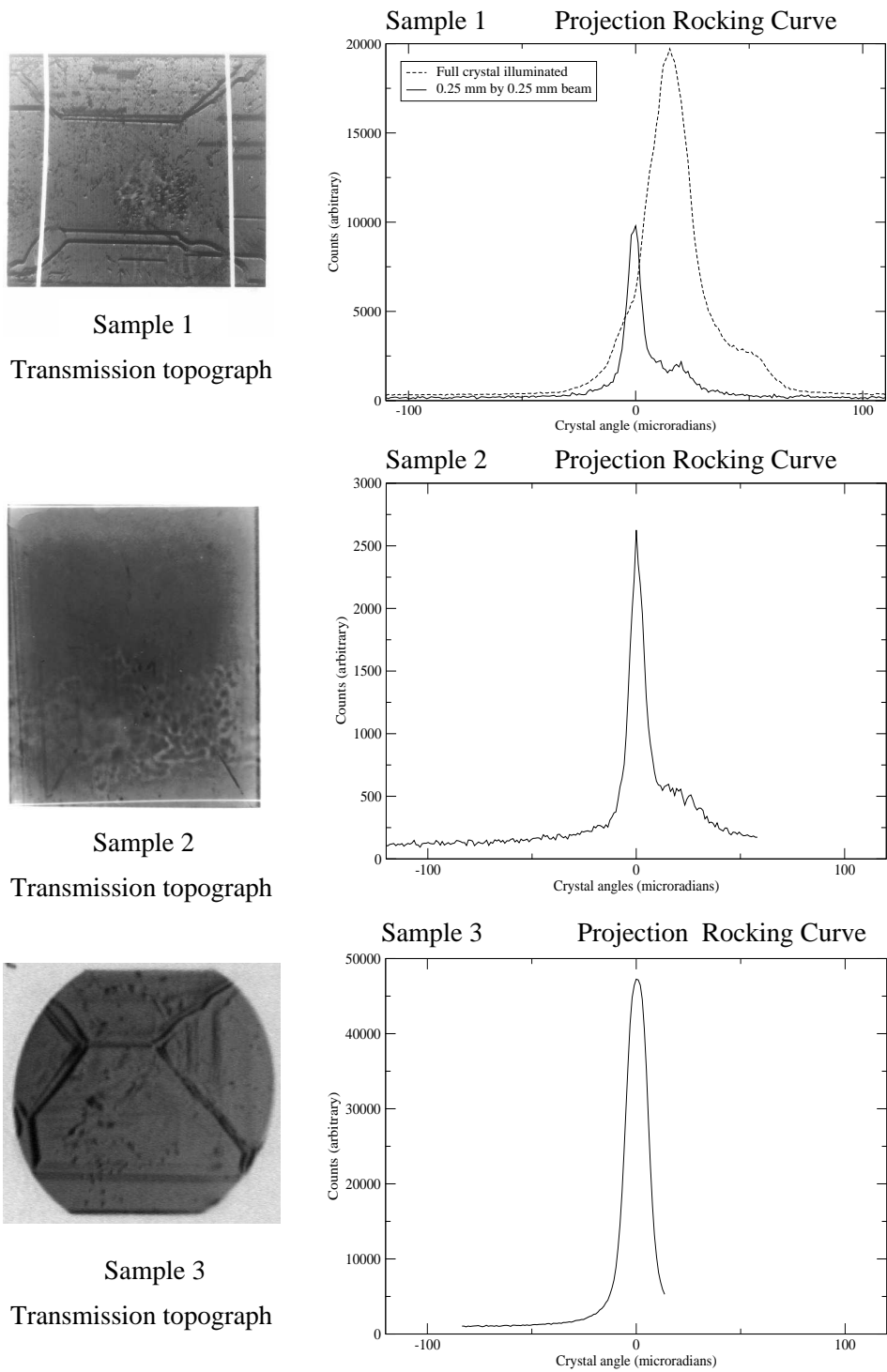


Fig. 5. Transmission topographs and rocking curves of samples 1, 2 and 3.

- see table 1. All three samples were chosen to have central regions in their topographs which are more or less featureless. Two rocking curves are shown for sample 1. The rocking curve with the dashed line corresponds to the illumination of the entire crystal by the X-ray beam. All the other rocking curves

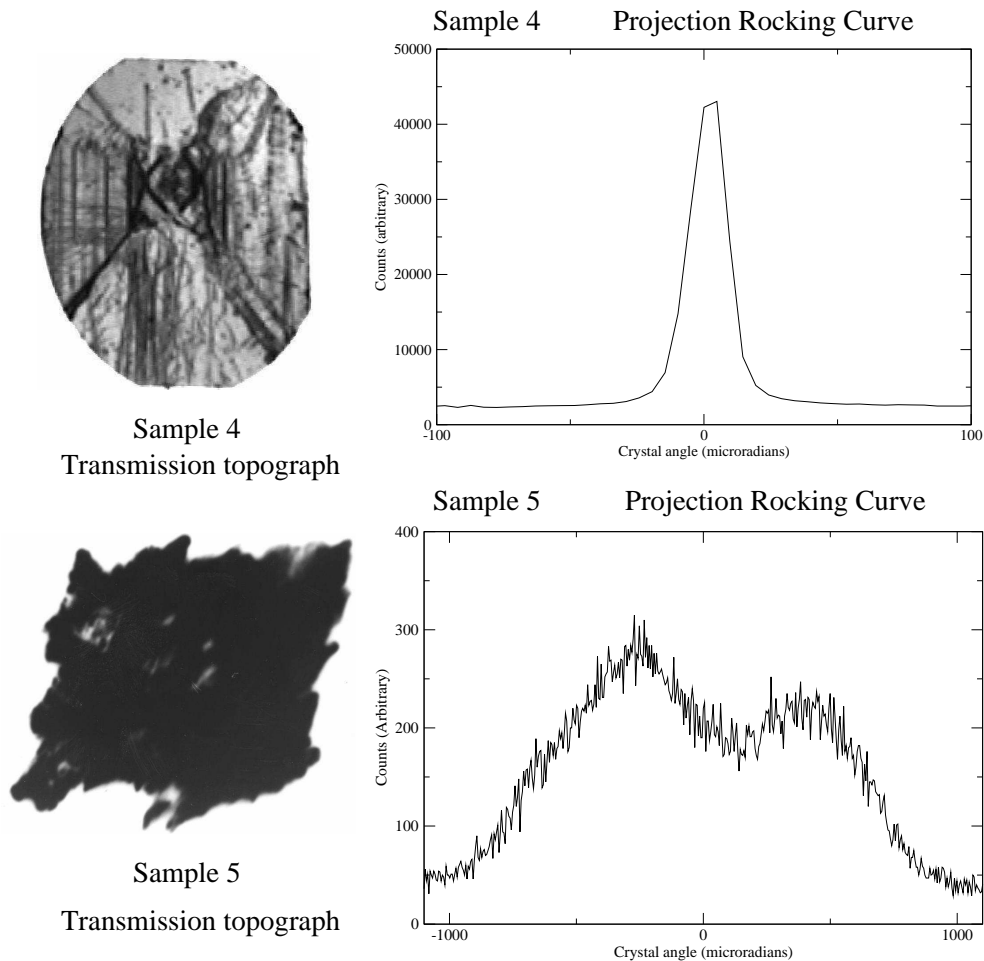


Fig. 6. Transmission topographs and rocking curves of samples 4 and 5.

shown correspond to the illumination of a central 0.25 mm square spot on the diamond. For samples 1 2, and 3 it is seen that a relatively featureless topograph correlates with a narrow rocking curve.

Figure 6 shows the topographs and rocking curves for samples 4 and 5. Sample 4 is a type I industrial synthetic whose topograph shows the imprint of the seed from which it was grown. It is seen that sample 5, a type II natural diamond, which shows considerable evidence of strain in the polarized light analysis, has a very broad rocking curve, and its topograph is severely misshapen.

Table 2 summarises the rocking curve results from these samples. It also gives rocking curve data for a sixth sample for which coherent bremsstrahlung spectra were measured using the Glasgow tagger at Mainz. The F.W.H.M.,  $W_{meas}$ , for the measured rocking curves can be compared with the theoretical F.W.H.M.,  $W_{th}$ , for an ideal lattice as predicted by dynamical X-ray scattering

Rocking Curves Widths							
<i>Sample</i>	<i>Type</i>	$\lambda$ ( $\text{\AA}$ )	<i>Plane</i>	$\theta_B$	<i>Beamsize</i> ( $\text{mm} \times \text{mm}$ )	$W_{th}$ ( $\mu\text{rad}$ )	$W_{meas}$ ( $\mu\text{rad}$ )
1	Ib	1	(004)	$33^\circ.9$	$0.25 \times 0.25$	5.4	6.7
2	Ib	1	(004)	$33^\circ.9$	$0.25 \times 0.25$	5.4	8.6
3	Ib	1.3	(022)	$31^\circ.1$	$0.25 \times 0.25$	11.9	12.4
4	Ib	1.3	(004)	$47^\circ.2$	$0.25 \times 0.25$	8.6	17.5
5	IIa	1	(004)	$33^\circ.9$	$0.25 \times 0.25$	5.4	$\sim 1200$
6	Ib	1	(004)	$33^\circ.9$	$0.25 \times 0.25$	5.4	30

Table 2

A table showing the rocking curve widths of the various samples.

theory ref(????). i.e.:

$$W_{th} = 2 \times \left( \frac{e^2}{m_e c^2} \right) \times \frac{\lambda^2 |F|}{\pi a^3 \sin 2\theta_B}$$

where  $\lambda$  is the X-ray wavelength,  $a$  is the lattice parameter for diamond, and  $\theta_B$  is the Bragg scattering angle.  $F = \alpha f$  where  $\alpha$  is an integer depending on the crystal reflection being used and  $f$  is the mean atomic scattering factor for electrons in carbon. The rocking curves are obtained by scattering from the (004) planes for the (001) diamonds, ie. for samples 1, 2, 4, 5, and 6, and from the (022) planes for sample 3, the (011) diamond (16). This is because the (001) and (011) planes have forbidden reflections and the (004) and (022) planes are the closest planes, with non zero structure factors, parallel to the face planes of the diamonds. The X-ray wavelengths were chosen to make  $W_{th}$  less than  $10 \mu\text{rad}$  for the (001) diamonds. For the (011) diamond  $W_{th}$  is slightly larger, having a value of  $\sim 12 \mu\text{rad}$ .

From the information presented in figures 5 and 6 and table 2, we can make the following observations:

- a) The small X-ray spot on samples 1, 2 and 3 gives sharp structure which is not much larger than the theoretical value for a perfect crystal. It is reasonable to conclude the full widths of the distributions (which are in the range from 6.7 to  $12.4 \mu\text{rad}$ ) give the angular ranges of the microcrystal axes in the mosaics of the samples. It is noticeable for sample 1 that this angular range increases when the whole crystal is measured as would be expected.
- b) The smooth rocking curve shape of sample 4 is consistent with this picture, but it has a more uniform range of crystal axis directions.
- c) Sample 5 shows a wide range of crystal axis directions, but there is no direct evidence whether this is produced by many good quality microcrystals, or, as

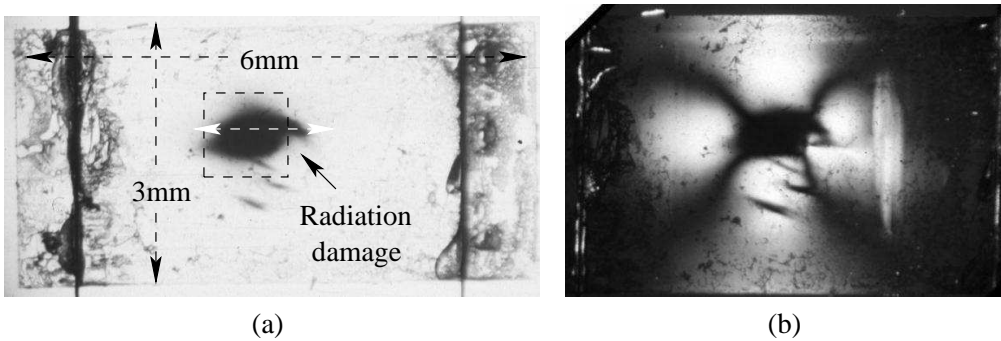


Fig. 7. Petrographic microscopy of the radiation damaged diamond sample without (a) and with (b) crossed polaroids.

the strain pattern seen in the polarized light picture suggests, that deformation of the lattice is a more probable explanation.

So far we have discussed techniques for measuring how closely the lattice structure of a diamond which has not been exposed to a high energy electron beam matches that of a perfect crystal. Using sample 6 we now describe the effect the incident electron beam has on a diamond radiator. To begin with we examine if the general shape of the coherent bremsstrahlung spectrum changes.

#### 4 Effect of the incident electron beam.

Figure 7 shows petrographic microscopy images of sample 6, without 7(a) and with 7(b), crossed polaroids. Both images show regions of damage where the electron beam (around  $10^{19}$  electrons in total) passed through the diamond. The dark vertical lines on the left and right of image (a) are supporting wires, and the dark areas around the wires are due to the glue holding the diamond to the wires changing colour after exposure to radiation.

The region of damage, which is outlined by the square box with dashed line edges in figure 7(a), was examined by measuring a set of reflection rocking curves along the white arrowed line in figure 7(a) at the Daresbury SRS with an X-ray beam collimated to a  $0.25 \text{ mm}$  square. In addition, coherent bremsstrahlung spectra were obtained for a series of points within the damaged region at the tagged photon facility in Mainz. The electron beam was focused to a spot approximately  $0.1 \text{ mm}$  in diameter.

The rocking curves are shown in figure 8. The rocking curves from the badly damaged region are much broader than those far from the damage centre. This means the damaged region has a much larger mosaic spread. From the rocking curves, we estimate the mosaic spread ( $\sigma_{\text{mosaic}}$ ) at the damage center is about  $120 \mu\text{rad}$  - see section 5 -, and far from the damage center about  $10 \mu\text{rad}$ . This indicates that away from the area which has been exposed to the

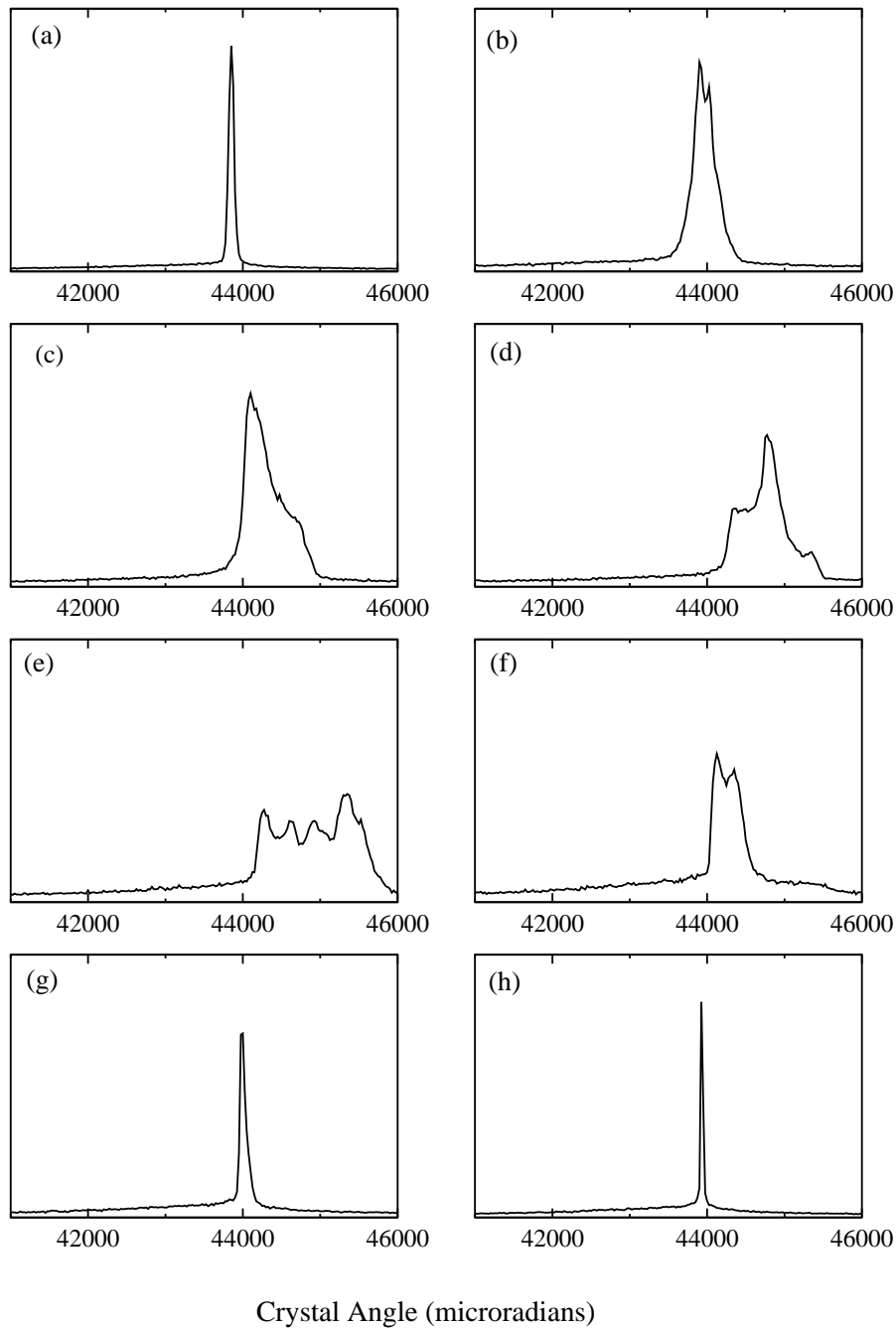


Fig. 8. Rocking curves at different positions along a line going through the radiation damaged center. For a-h, each point has a distance from the damage center of: -0.75mm, -0.50mm, -0.25mm, -0.0mm, 0.25mm, 0.50mm, 0.75mm, 1.0mm

electron beam, the diamond has a lattice structure which is almost perfect. The coherent bremsstrahlung spectra from the damaged region were examined by firstly looking for evidence that the damage could have changed the ratio of coherent to incoherent bremsstrahlung between the damaged and undamaged regions of the sample.

The bremsstrahlung from a crystal has a coherent part and an incoherent part.

The incoherent part also contains a crystal contribution and an electron contribution. Using a computer programme developed by Natter (2) which calculates the bremsstrahlung from both a diamond single crystal and an amorphous radiator, we find the best theoretical fit to an experimental bremsstrahlung spectrum from a diamond radiator by adding an adjustable extra incoherent component to the theoretical intensity and minimize  $X^2$ , where

$$X^2 = (I_{me} - (\alpha I_{dt} + \beta I_{nt}))^2.$$

$I_{me}$  is the measured intensity of diamond bremsstrahlung,  $I_{dt}$  is the calculated theoretical intensity of diamond bremsstrahlung, and  $I_{nt}$  is the calculated theoretical amorphous intensity.  $\alpha$  and  $\beta$  are two parameters, which are varied to minimize  $X^2$ , and hence find the best fit. The incoherent contribution  $I_{nt}$  uses the theoretical approach of Hubell (17).

No.	1	2	3	4	5	6	7	8	9	10
$x(mm)$	-1.5	-1.2	-0.9	-0.6	-0.3	0	0.3	0.6	0.9	1.2
$\mu$ (%)	7.8	8.5	9.4	9.9	8.1	9.0	11	9.2	9.4	10
$X^2$	3.35	2.38	3.13	2.20	3.19	3.34	3.93	3.00	3.04	4.13

Table 3

Least squares simulation results;  $\mu = \beta/\alpha$  and  $x$  is the position along the white arrowed line shown in figure 7(a). The damage centre is defined by  $x=0$ .

The results of fitting the experimental bremsstrahlung spectra from sample 6 are summarized in table 3.

It is found that, after introducing the extra incoherent background, the fitted theoretical results agree well with the measured spectra. The amount of extra incoherent background is estimated by the parameter  $\mu = \beta/\alpha$ . The spectra were taken at different points along a line going through the radiation damaged region, where the  $x = 0$  mm point is located at the damage center. The bottom row in table 3, lists the values of  $X^2$  for different positions. The consistency of the values for  $X^2$  demonstrates that the confidence level of the fits does not vary significantly across the damaged region. Although, in the damaged region, the beam electrons caused many defects, as can be observed from the discoloration around the damage center and from the wide rocking curve widths, there is no significant change in the amount of extra incoherent background required between the damaged and the undamaged regions. This means the disorder caused by the radiation at the dose level and electron beam energy used, has little effect on the shape of the incoherent bremsstrahlung spectrum. It is probable that the extra incoherent background indicated in table 3 is due to limitations in the theoretical description of the bremsstrahlung spectrum from diamond.

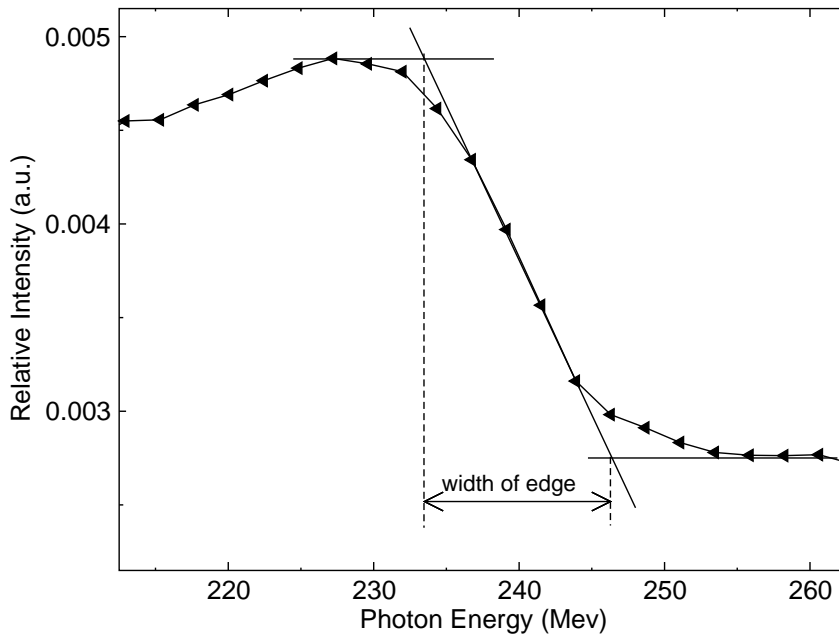


Fig. 9. Definition of the width of the coherent peak edge.

Another factor that affects the bremsstrahlung background is the radiator temperature (3). The background increases with temperature, and we find the extra background in table 3 can be accounted for by assuming the radiator temperature increases to about 800  $K$ . At present, the diamond temperature can not be measured directly during the bremsstrahlung measurements, but it is possible to estimate an upper limit for the temperature. In our experiments, the diamond radiator is glued to two vertical tungsten wires by an organic glue. Since a temperature higher than 500  $K$  will destroy the glue, and the diamond has never separated from the wires, the radiator temperature is not very high. Theoretical predictions have also estimated that the radiator temperature does not exceed 400  $K$  in normal conditions(8). Hence, it is unlikely the radiator temperature influenced the incoherent part of the bremsstrahlung significantly.

Though crystal imperfections caused by the electron beam have little effect on the incoherent bremsstrahlung, we have observed some effects on the coherent part. We find that for the radiation damaged diamond (sample 6) and also a plastically deformed diamond, which is not described explicitly in the present paper, the width of the coherent edge becomes broader. The way we define the coherent edge width is illustrated in figure 9. The two straight lines parallel to the horizontal axis go through the maximum and minimum of the coherent edge, and the third line defining the slope of the edge intersects the two horizontal lines. These two intersections define a line segment, the projection of which onto the horizontal axis defines the width of the edge. Figure 10 shows the width of the edge for different positions within the damaged region - see figure 7(a). The points are defined by  $x$  and  $z$  co-ordinates where the  $x$  axis lies along the white arrowed line shown on figure 7(a) and the  $z$  axis is at right



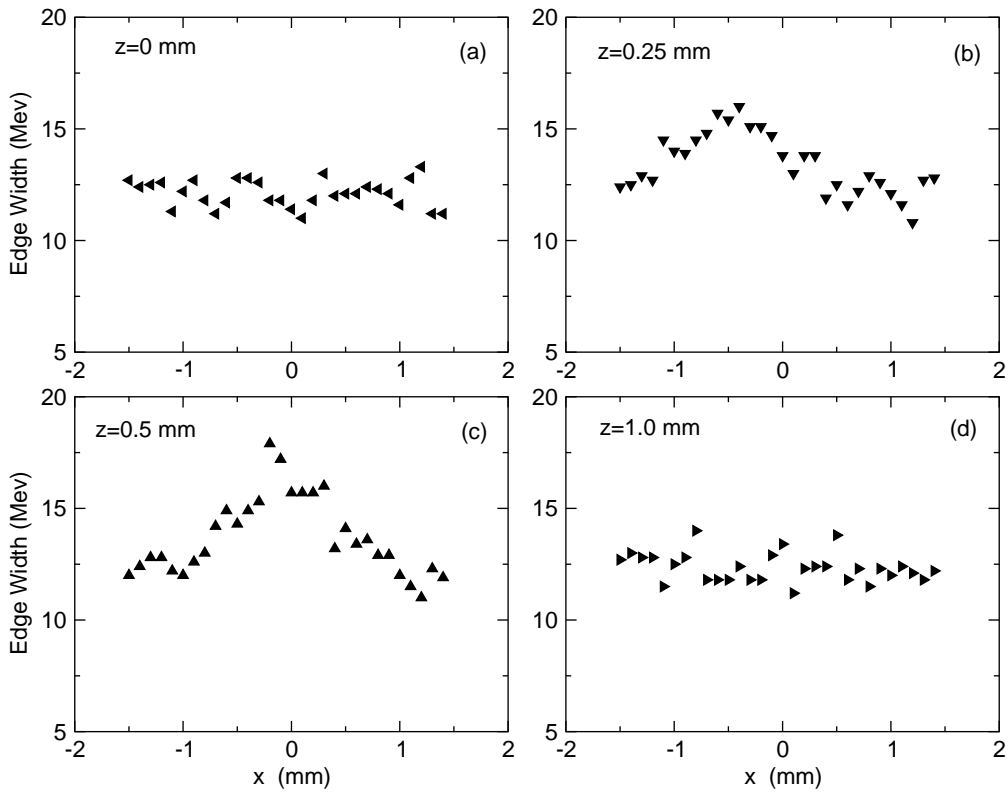


Fig. 10. The variation of the width of the coherent edge of sample 6 with  $x$  and  $z$  position. Referring to figure 7 the  $x$ -axis is horizontal and the  $z$ -axis vertical, with the origin at the damage center. When  $z=0.25\text{mm}$  and  $0.5\text{mm}$ , the  $x$  scan goes through the damaged region.

angles to the line. It is seen that in figures 10 (b) and (c), the width changes with  $x$ , and reaches a maximum at about  $x=0\text{ mm}$ . However, in figures 10 (a) and (d), the width of the edge is almost constant. The  $x$  scans at  $z=0.25\text{ mm}$  and  $0.5\text{ mm}$  go through the radiation damaged region, whereas the  $z=0\text{ mm}$  and  $1\text{ mm}$  scans are outwith the damaged region.

Comparing the rocking curve measurements with the bremsstrahlung spectra for the damaged region in sample 6 we find a large mosaic spread corresponds to a broader coherent bremsstrahlung peak edge, which is consistent with the prediction of Timm (3). By referring to figure 10, it appears that there is an underlying coherent edge width of around  $12.5\text{ MeV}$  present across the whole of the diamond, but in the damaged region this increases to around  $15\text{ MeV}$ .

## 5 Discussion.

Because mosaic spread, multiple scattering and beam divergence have similar effects on the diamond coherent bremsstrahlung spectrum, we should take

them all into account. The total effective angular spread( $\sigma_{total}$ ) is given by

$$\sigma_{total}^2 = \sigma_{mosaic}^2 + \frac{1}{2}\sigma_{sc}^2 + \sigma_{beam}^2$$

where  $\sigma_{mosaic}$ ,  $\sigma_{sc}$  and  $\sigma_{beam}$  refer to the mosaic spread, multiple scattering and beam divergence respectively. In the equation we use the plane projected multiple scattering formula which is a factor of  $\frac{1}{\sqrt{2}}$  less than the space formula since it is appropriate for combining Gaussian distributions. We also take an average throughout the thickness of the diamond to describe the multiple scattering. This introduces the factor of 1/2 since multiple scattering varies predominantly as the square root of the thickness.

For the 855 MeV Mainz electron beam the bremsstrahlung characteristic angle is around 600  $\mu rad$ , and for the 100  $\mu m$  thick diamond (sample 6), the average r.m.s. multiple scattering angle is about 235  $\mu rad$ . The beam divergence was believed to be less than 100  $\mu rad$  in our experiments(9), and for the present analysis we use a value of 50  $\mu rad$ . From figure 8(e) at the center of the damaged region, the rocking curve seems to consist of at least 4 overlapping peaks each of which has a width comparable to the widths of the most prominent features in figures 8(b),(c),(d) and (e). Since the main X-ray beam at Daresbury is collimated to a 0.25 mm square and the Mainz electron beam has a diameter of 0.1 mm, the X-rays are able to sample the damage resulting from several closely spaced electron beam spots simultaneously. This could explain the shape of the rocking curve in figure 8(e). The mosaic spread in the damaged region is estimated from the average width of the most prominent structures in the rocking curves associated with the damaged region. Around the damage center the mosaic spread is estimated to be about 120  $\mu rad$  and about 10  $\mu rad$  away from the damage center. Hence the total effective angular spread is about 270  $\mu rad$  for the damage center and about 240  $\mu rad$  away from the damaged region. Consequently, for the Mainz beam energy and the 100  $\mu m$  radiator used for the measurements, the overall angular spread does not change too significantly even although the mosaic spread shows such a large difference between the damaged and undamaged regions. This is due to the large multiple scattering contribution from the 100  $\mu m$  thick diamond. By referring back to figure 3(a), we can estimate the r.m.s. spread in the upper edge energy of the coherent peak at  $E_\gamma \sim 240 MeV$  from the angular changes of 240  $\mu rad$  and 270  $\mu rad$ . Values of around 6.5 and 7.3 MeV are found. To make a comparison with the results in figure 10, the coherent photon spectrum must be folded with the distribution of the edge energies. We find that the width  $W$  of the coherent edge is given by  $W = (2.3 \pm 0.3)\sigma$  where  $\sigma$  is the r.m.s. spread in energies. Values for  $W$  of  $15.0 \pm 2.0 MeV$  and  $16.8 \pm 2.2 MeV$  are found for the undamaged and radiation damaged regions respectively. Although these are slightly larger than the coherent edge widths of  $12.5 \pm 1.0 MeV$  and  $15.0 \pm 1.0 MeV$  for the undamaged and damaged regions shown in figure 10, the agreement is sufficiently close to provide a qualitative explana-

tion of the results shown in figure 10.

From figure 8, it also appears that the positions of the rocking curves change in a consistent way. ie: away from the damage centre, (a) and (h), the rocking curves have essentially the same position, but in moving towards the damage centre the curves shift towards the right, until at the center, (e), the left hand edge of the curves has moved by around  $430 \mu rad$ . If we interpret this as evidence that the orientation of the rocking curve scattering planes has been altered by half this amount ( $215 \mu rad$ ), the coherent edge of the bremsstrahlung spectrum would be shifted by around 6 Mev, which is not observed. Another explanation of the effect, which is discussed more fully towards the end of this section in a related context, is that the radiation damage has produced a macro deformation throughout the volume of the crystal which has altered the inter-atomic plane distance  $d$ . From the Bragg equation,  $d$  will change by a factor of  $\sim 3 \times 10^{-4}$  if the scattering angle changes by  $\sim 215 \mu rad$ . Furthermore, since the rocking curves for the damaged region have larger values for the goniometer setting, the Bragg angle actually decreases and hence  $d$  increases slightly. The reciprocal lattice vector will change by the same factor as  $d$ . Since the condition for coherent bremsstrahlung production is that the momentum transfer associated with the bremsstrahlung process equals the reciprocal lattice vector of the scattering planes, the coherent edge will shift. This is apparent from the equation linking the minimum longitudinal momentum transfer  $q_l$  to  $k_C = \frac{E_{\gamma}^{edge}}{E_0}$  the fractional photon energy of the coherent edge. ie:  $q_l = \frac{1}{2} E_0 \frac{k_C}{1-k_C}$ . It follows that  $\frac{\delta k_C}{k_C} = (1 - k_C) \frac{\delta q_l}{q_l}$  where  $\delta k_C$  is the change in  $k_C$  resulting from a change  $\delta q_l$  in  $q_l$ . This means there will be a shift in the position of the coherent edge at  $\sim 240 MeV$  of approximately  $0.05 MeV$  due to the estimated change to the inter-atomic plane distance. However, if  $d$  changes, the volume of the crystal and the orientations of the lattice planes relative to those of an undamaged crystal will be affected. Referring to figure 8, the maximum shift in the rocking curves takes place over a distance of  $\sim 0.5 mm$  on the crystal. The change of  $3 \times 10^{-4}$  in  $d$  will produce a change in the thickness of the diamond of  $\sim 0.03 \mu m$  leading to an average angular change of  $\sim 30 \mu rad$  in the orientation of the planes for a photon energy  $\sim 240 MeV$ . This level of angular distortion of the lattice planes will produce a shift of  $\sim 0.8 MeV$  in the position of the bremsstrahlung coherent edge at  $\sim 240 MeV$ . As will be shown later, shifts in the position of the coherent edge have been observed for the radiation damaged diamond which are comparable with the estimated magnitudes of the shifts originating from a change in  $d$  discussed above.

To summarise our interpretation of the measurements shown in figure 8, we think there are two main effects which are interlinked. Firstly, there is a local increase in the mosaic spread of the diamond around the beam spot which leads to a broadening of the coherent edge, and secondly, a macro strain is set up in the diamond resulting in a small increase in the inter-atomic plane separation.

We shall now consider some of the implications the preceding discussion has for higher electron beam energies. Since the characteristic angle for a higher electron beam energy is much smaller, the shape of the coherent edge is much more sensitive to the beam divergence, multiple scattering, and mosaic spread. For example for 12 *GeV*, the characteristic angle is about 42  $\mu rad$ . Hence, if we use a beam divergence of 15  $\mu rad$ , which will be an average value for the GlueX project, and have a 40  $\mu m$  thick diamond which has an average plane projected r.m.s. multiple scattering angle of about 10  $\mu rad$ , then if the mosaic spread changes from 10  $\mu rad$  to 120  $\mu rad$  - the values used to study radiation damage in sample 6 - the total angular spread will change from  $\sim 20 \mu rad$  to  $\sim 120 \mu rad$ . Referring to figure 3(b) an angular spread of 120  $\mu rad$  would result in an r.m.s. spread in the upper edge energy of the coherent peaked at  $E_\gamma \sim 8 GeV$  of around 120 *MeV*. When the coherent photon spectrum is folded with the distribution of edge energies we find the width *W* of the coherent edge would have estimated values of  $46 \pm 6 MeV$  and  $270 \pm 36 MeV$  for undamaged and damaged parts of the crystal. The resulting smearing of the coherent bremsstrahlung peak from a damaged region would lead to a substantial decrease in the degree of linear polarisation, particularly if the photon beam is highly collimated (8).

For the GlueX experiment we now estimate how long it would take for this level of damage to occur. We assume the level of damage is proportional to the number of electrons passing through unit area of the diamond. The GlueX 12 *GeV* electron beam spot at the radiator is designed to have a transverse size of  $\sim 1.7 mm$  r.m.s. and a vertical size of  $\sim 0.5 mm$  r.m.s. Since the electron beam spot used for coherent bremsstrahlung production at Mainz has a diameter  $\sim 0.1 mm$  r.m.s. the area of the GlueX beam spot will be  $\sim 84$  times that of the beam spot at Mainz. If we assume the total estimated number of  $10^{19}$  electrons through the Mainz diamond consisted of  $\sim 5 \times 10^{17}$  electrons through 20 separate beam spots, then the number of *electrons/mm<sup>2</sup>* responsible for the level of radiation damage observed was  $\sim 6.4 \times 10^{19} electrons/mm^2$ . Across the area of the GlueX beam spot this translates to a total of  $\sim 4.2 \times 10^{19}$  electrons. If GlueX has a full intensity beam current of 3  $\mu A$  the experiment could run for  $\sim 1$  month at full intensity before the diamond would experience radiation damage similar to that of the Mainz crystal. However, this level of radiation damage would be too high for GlueX and it will be essential to monitor the flux of collimated photons carefully and limit the exposure of the diamond to the electron beam.

As mentioned earlier, we have found possible evidence of a slight volume change associated with radiation damage within the crystal resulting from the inter-atomic plane distance having been altered. Volume changes have already been observed by other authors studying radiation effects (18). The petrographic microscopy of radiation damaged diamond typically shows a stress pattern which has a uniform strain field with 4-fold symmetry which is like the stress caused by a large inclusion. Since this is exactly the form of the petrographic image shown in figure 7(b), this provides further evidence from

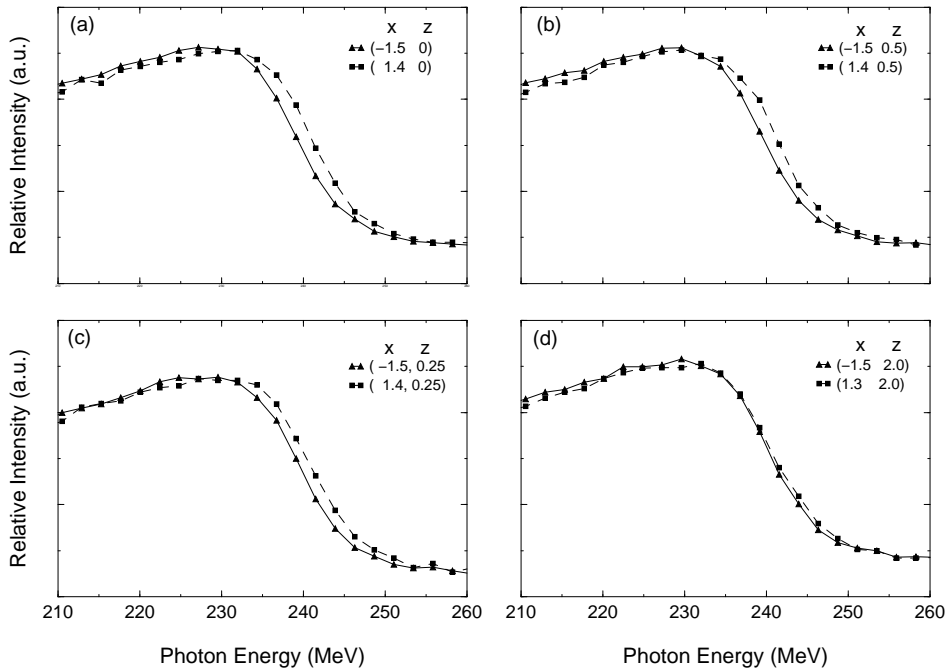


Fig. 11. Relative intensity  $(I^{coh} + I^{incoh})/I^{incoh}$  of bremsstrahlung spectra for the sample 6 diamond at different positions. Referring to figure 7 the x-axis is horizontal and the z-axis vertical, with the origin at the damage centre.

petrographic microscopy that sample 6 has a macro deformation.

We have argued that for sample 6 there should be a coherent peak shift of around an MeV associated with changes to the inter-atomic plane distance. This phenomenon is readily observed experimentally for sample 6 and is illustrated in figure 11, which consists of four diagrams, each showing two bremsstrahlung spectra at two different points on the diamond. The coordinates of these points are shown on the top right corner of each diagram. Each pair of spectra has a common z co-ordinate, but x co-ordinates that are symmetrically placed with respect to the damage center. The spectra were taken using the same electron beam incident angle with respect to the diamond, and hence each spectrum should have the same peak position. However, from figures 11 (a), (b) and (c), a difference between the two bremsstrahlung peak positions of around 1 to 2 MeV is seen, which is close to the value predicted earlier in the paper. For figure 11 (d), the peak position difference is much smaller. The two points in figure 11 (d) are farthest from the damage centre, where the effect of the macro stress is expected to be smaller.

## 6 Conclusions.

In this paper we have considered how the angular spread of an electron beam passing through a diamond is affected by the divergence of the beam, the thick-

ness of the crystal and the presence of defects in the lattice. Independently of the beam energy the optimum thickness for a diamond radiator is around  $40 \mu\text{m}$ . We have demonstrated that the techniques of petrographic microscopy, X-ray topography and measuring X-ray rocking curves provide complementary information about the crystal lattice. ie: featureless petrographic and topographic images seem to correspond to narrow rocking curves and are typical of diamonds with few lattice defects. Furthermore, it is possible to obtain diamond specimens of very high quality from synthetic industrial diamonds. We have also discussed the effects of the incident electron beam on coherent bremsstrahlung production. The following effects have been found for sample 6, the radiation damaged diamond.

- (1) The atomic disorder resulting from defects caused by the incident electron beam does not have a significant effect on the general shape of a coherent bremsstrahlung spectrum, even though the corresponding rocking curve width is significantly broadened by radiation damage.
- (2) The crystal imperfections cause the coherent edge width to become broader.
- (3) There is a uniform strain caused by an associated volume expansion leading to a small coherent bremsstrahlung edge shift across the region of strain. We conclude that this is caused by changes to the inter-atomic plane distance which results in a small increase in the volume of the crystal.

For a  $12 \text{ GeV}$  electron beam, a thin high quality diamond crystal with a small mosaic spread is essential. In particular, for a  $40 \mu\text{m}$  diamond, if the mosaic spread changes by a factor of 12 from  $10$  to  $120 \mu\text{rad}$  due to radiation damage, it is estimated the width of the coherent edge at  $8 \text{ GeV}$  will change by a factor of 6, from around  $46 \text{ MeV}$  to around  $270 \text{ MeV}$ . Since the resulting reduction in the degree of linear polarisation of collimated coherent bremsstrahlung photons would be significant, the level of damage from the electron beam should be closely monitored by noting if the width of the coherent edge increases.

At the beginning of the paper, we stated that one of our aims was to investigate if there was a simple and inexpensive assessment technique which could provide sufficient information to determine how well a diamond would perform as a radiator. Ideally, the hope would be that a featureless image from petrographic microscopy would be sufficient. Unfortunately, this is probably not the case as is demonstrated in figures 12 and 13. Figure 12 shows transmission topographs of 4 slices, each  $100 \mu\text{m}$  thick, cut from a single synthetic diamond (which has not been discussed previously in the paper). The corresponding petrographic images are essentially the same as the topographs. The progression from (a) to (d) illustrates how the features in the topographs change with distance from the seed crystal. Figure 12(d), which is furthest from the seed, appears relatively featureless, but the rocking curve for 12(d), shown in figure 13, reveals a complex mosaic structure which extends across an angular range of  $\sim 150 \mu\text{rad}$ , so that this diamond would be unsuitable for

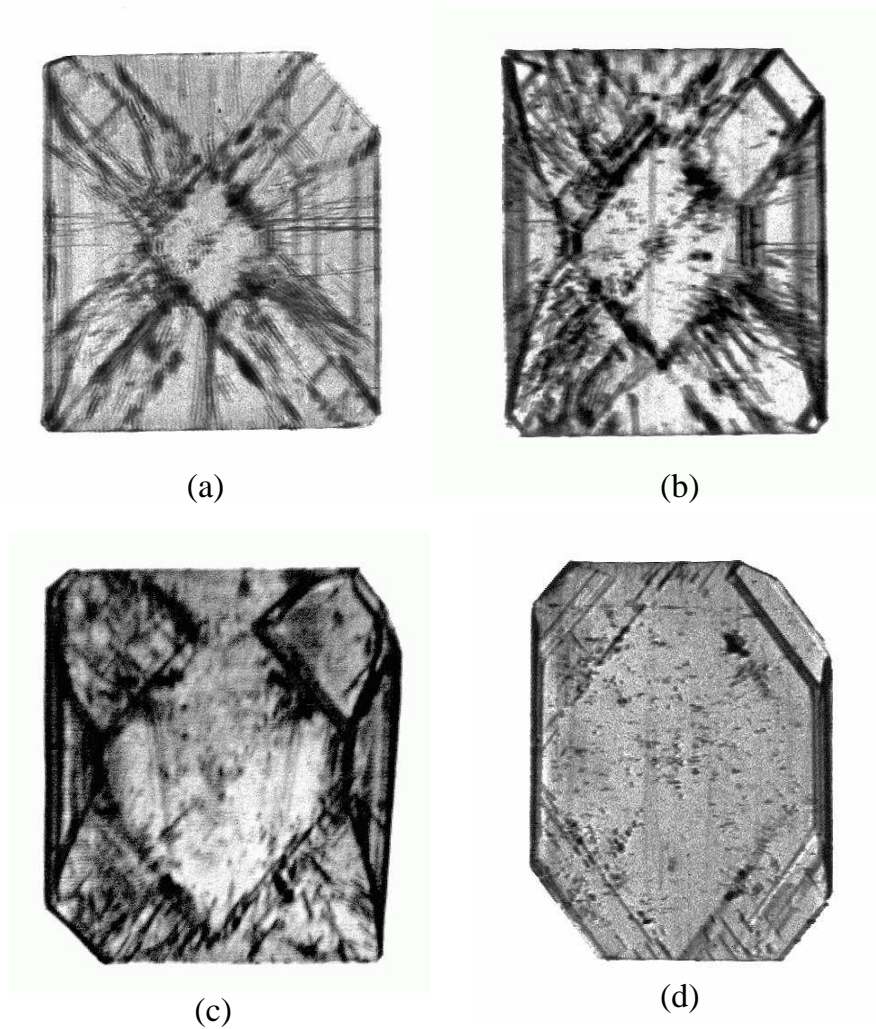


Fig. 12. Transmission topographs for four  $100\ \mu\text{m}$  sections cut from a single synthetic diamond

GlueX.

On the other hand, the polarized light image shown in figure 4(a) is for one of a set of 3 slices cut from another single synthetic diamond. All 3 slices have very similar petrographic images and transmission topographs and narrow rocking curves. Consequently, if it is possible to obtain several slices from the same synthetic diamond and they all have similar featureless petrographic images, then there is probably no need for an X-ray analysis. However, for a diamond on its own, irrespective of whether it is natural or synthetic, it would be sensible to carry out an X-ray analysis. Furthermore, since the quality of a diamond radiator being used in an experiment with linearly polarised photons will determine the degree of linear polarization of the photon flux, it would be inadvisable to use a radiator which had not received a thorough assessment. This is particularly important if beam energies greater than several  $\text{GeV}$  are being used.

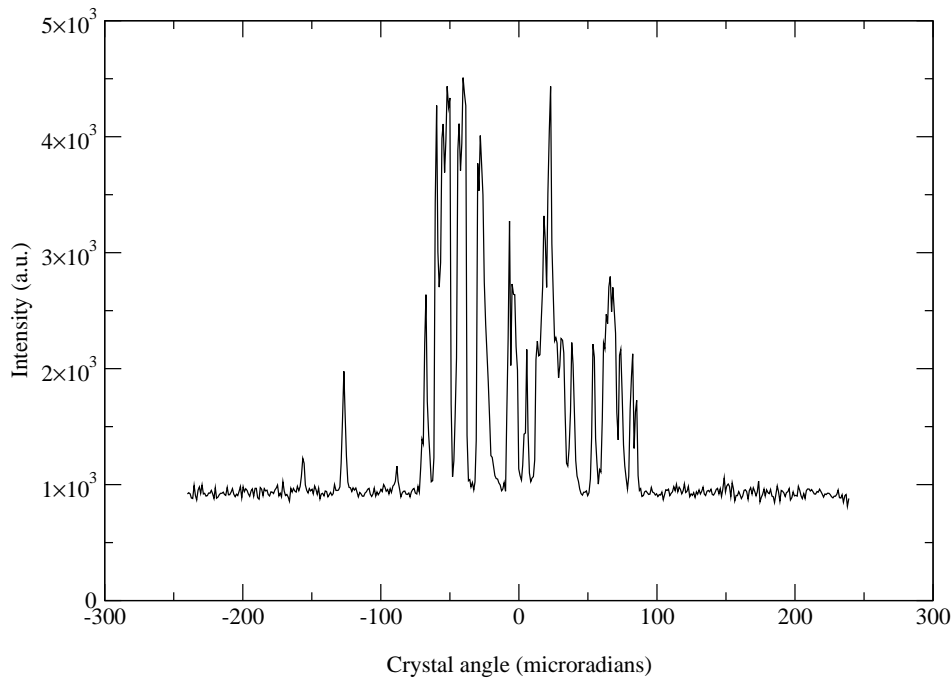


Fig. 13. Rocking curve for diamond section with topograph shown in fig 12(d)

The authors acknowledge support of this work by the Engineering and Physical Sciences Research Council and would also like to thank the Director of the Synchrotron Radiation Source at Daresbury and the Director of the Institut für Kernphysik at Mainz University. They also acknowledge the help received from the manager of station 7.6, Dr. David Laundry, at the SRS, Daresbury and are grateful to Element 6 for their expertise in polishing the diamond samples.

## References

- [1] D. Lohmann *et al.*, *NIM A* **343** (1994) 494.
- [2] A. Natter, *A Coherent Bremsstrahlung Simulation Code*, Private communication, (2001).
- [3] U. Timm, *Fortschritte der Physik* **17** (1969) 765.
- [4] G. D. Palazzi, *Rev. Mod. Phys.* **49** (1968) 611.
- [5] G. Davies, *Diamond*, Adam Hilger, (1984).
- [6] I. Anthony *et al.*, *NIM A* **301** (1991) 301.
- [7] S. J. Hall *et al.*, *NIM A* **368** (1996) 698.
- [8] The Science of Quark Confinement and Gluonic Excitations. *GlueX/Hall D Design Report*, Version 4, Jefferson Laboratory (2002).
- [9] F. Rambo *et al.*, *Phys. Rev. C*, **58** (1998) 489.
- [10] L. Montanet *et al.*, *Phys. Rev. D*, **50** (1994) 1173.
- [11] B. K. Tanner, D. K. Bowen, *High resolution X-ray diffractometry and topography*, Taylor and Francis, (1998).



- [12] B. K. Tanner, *X-ray diffraction topography*, Pergamon, 1976.
- [13] M. M. Woolfson, *An Introduction to x-ray Crystallography* Cambridge University Press.
- [14] C. G. Darwin, *Phil. Mag.*, **43** (1922) 800.
- [15] K. Livingston, *An Alignment Technique for Diamonds used in Coherent Bremsstrahlung Experiments*, Private communication, (2002).
- [16] S. Elliott, *The Physics and Chemistry of Solids*, John Wiley and Sons, (1998).
- [17] J. L. Hubbell, Spectrum of thin Target Bremsstrahlung bounded by a forward circular Cone, *J. Appl. Phys.* , **30** (1959) 981.
- [18] R. Kalish, A. Reznik, et al. *Nuclear Instruments and Methods B* ,**148** (1999) 626-633.